Microcavity Laser Emissions Based on Double Hetero-Structure by Locally Modulated Photonic Crystal Waveguide

Chia-Ho Chen, Tsan-Wen Lu, and Po-Tsung Lee, *Member, IEEE*

***Abstract*—In this paper, we design a microcavity with vertical and in-plane emissions by applying double hetero-structure with mode-gap confinement in photonic crystal waveguide. The hetero-structure is formed by modulating the waveguide width locally by slightly shifting the positions of several nearest air-holes outward. By numerical calculations, we simulate the basic mode profiles and quality (Q) factors of each resonance mode. After optimizing the cavity, high simulated Q factor of 110 000 is obtained. From the well-fabricated devices, we observe the lasing emissions with Q factor of 3200 at wavelength of 1593 nm from both vertical and in-plane directions and address the lasing mode by comparing the measured results with the simulated ones. From the simulated heat transition behaviors by finite-element method, we observe the better heat dissipation provided by the waveguide region in this microcavity. This microcavity laser with locally modulated design could be potentially served as a light source with less influence on the nearby components in photonic integrated circuits.**

***Index Terms*—Hetero-structure photonic crystal, microcavity, semiconductor laser.**

I. Introduction

FOR past decades, microdisk lasers [1] have been regarded as a key role in realizing photonic circuits due to their excellent properties, including disk-edge emissions, high quality (Q) factors, and so on. Particularly, the disk-edge-emitting property makes it possible for researchers to guide in or out the light emission by employing external waveguides, which shows high potential in constructing photonic circuits. However, when people minimize the device size to achieve condensed photonic integrated circuits (PICs), dramatic performance degradation arisen from the increasing bend losses becomes a huge problem. In recent years, various photonic crystals (PhCs) with photonic band-gap (PBG) effect have overcome this obstacle in constructing condensed PICs. Until now, various active PhC-based devices have been proposed and demonstrated, including defect microcavity [2]–[4] and defect-free (band-edge emitting) lasers [5], [6] aiming at various excellent properties, and the PhC microcavity laser has been widely expected as a potential light source in PICs. However, most reported PhC defect microcavities are mainly with vertical emissions and not suitable for integration or applying in planar PICs. Although one can lead out the vertical emission and convert it into planar system by optical microfibers [7], [8], this approach still increases the complexity in design, optical losses caused by coupling, and costs in module. Intuitively, microcavity design directly fused with waveguide would be a better approach in achieving high efficiency and low loss active in-plane emission light source in PICs. The most significant advantage of such structure is the light input and output can be achieved without extra external waveguides or other components. To form the light-localization region in a PhC waveguide, recently, various hetero-structure PhCs [9] with mode-gap effect have been proposed and investigated. Generally, the hetero-structure in a 2-D PhC waveguide can be achieved by locally varying PhC lattice constant [10], [11], air-hole size [12], lattice symmetry level [13], waveguide width [14], [15], and material index [16], which have been widely considered and reported in passive devices. However, only few literatures related to this kind of active device have been reported [17]–[20].

In the second part of this report, we will introduce a microcavity design based on three-row-missing (named W3) PhC waveguide with double hetero (DH) structure formed by slightly shifting the lattice positions of nearest air-holes of the waveguide locally. The mode-gap effect of the proposed hetero-structure PhCs is confirmed by plane-wave expansion (PWE) method. Then we investigate and optimize the modal properties and Q factors of the microcavity by 3-D finite-difference time-domain (FDTD) method. In the third part, by a series of dry- and wet-etching processes on InP-based semiconductor material, the real devices are well fabricated. From the measurements, the lasing actions in vertical and in-plane directions are both obtained, and by the measured results from these two directional emissions, we identify the lasing mode by comparing them with the simulated results. We also investigate and discuss the better heat dissipation of proposed microcavity due to the presentation of PhC waveguide by finite-element method (FEM).

II. Double Hetero-Structure Photonic Crystal Microcavity and Simulated Modal Properties

As we illustrated before, in 2-D PhC waveguides, one can create a defect-region to confine the light by applying DH

Manuscript received October 08, 2008; revised March 19, 2009 and May 12, 2009. First published June 02, 2009; current version published August 28, 2009. This work was supported by Taiwan's National Science Council (NSC) under ContractsNSC-97-2120-M-009-004 and NSC-95-2221-E-009-056.

The authors are with the Department of Photonics and Institute of Electro-Optical Engineering, National Chiao Tung University, Hsinchu 300, Taiwan (e-mail: jaherchen@hotmail.com; ricky.eo94g@nctu.edu.tw; potsung@mail.nctu.edu.tw).

Color versions of one or more of the figures in this paper are available online at http://ieeexplore.ieee.org.

Digital Object Identifier 10.1109/JLT.2009.2024010

structure formed by changing lattice parameters locally. With this local variation of lattice parameter, the frequency of propagating mode in this waveguide region will be shifted. Due to this shifting, the mode propagating in this local region will be forbidden when propagating into the original waveguide, which is known as the mode-gap effect. Among the approaches mentioned above in forming the PhC hetero-structure, locally modulating the waveguide width would be a better choice than varying the whole lattice structure [10], [11], [19], [20] when applied in condensed PICs. Especially for fusing with other PhC components, this local design will have less influence on modal properties of other nearby components. According to this concept, in our design shown in Fig. 1(a), the six nearest air-holes (red circles, denoted as air-holes A) of the PhC W3 waveguide are shifted a distance d_A outward and form the microcavity region, which is named PhC DHW3 microcavity with a larger waveguide width. Actually, the waveguide width can also be modulated by other approaches, for example, locally tuning the nearest air-hole radius [12]. However, controlling the air-hole size precisely in real fabrication process is more difficult due to the proximity effect in electron-beam lithography (EBL). This PhC DHW3 microcavity formed by simply shifting the nearest lattice positions reveals a very local and simplified design compared with other PhC DH microcavity designs in refs. [18]–[20]. It should also be noted that we choose PhC W3 waveguide instead of W1 waveguide for two purposes: 1) to reduce thermal problems in active laser device due to large waveguide size and 2) to expect for large laser emissions. Although there will be more resonance modes in DHW3 microcavity than in DHW1 microcavity, only one relatively high Q mode in simulation and single mode lasing in experiments are obtained from the DHW3 microcavity design in the following sections of this report.

To understand the modal properties in a PhC DHW3 microcavity, PWE and FDTD methods are applied in our simulations. The thickness and refractive index of PhC membrane are set to be 220 nm and 3.4, which correspond to an InGaAsP membrane supporting single fundamental mode. The lattice constant (a) and air-hole radius (r) over a (r/a) ratio are set to be 480 nm and 0.28 to 0.36. The simulation domain and the grid size are $30a$ (x-direction) $\times$ $30a$ (y-direction) $\times$ $8a$ (z-direction) and $a/20$, respectively. The numbers of PhC lattice periods in x and y directions are set to be large enough, both are 14, to provide sufficient in-plane PBG confinements. The PhC waveguide with DH structure shown in Fig. 1(a) is formed by initially setting the shifting distance d_A to be $0.1a$. We first calculate the transverse-electrical (TE) polarized (E-field lies in x-y plane, that is, E_x and E_y components) photonic band diagram of PhC W3 waveguide without and with lattice shifting by PWE method when r/a ratio is 0.3, as shown in Fig. 1(b). For example, from band-2 and band-2′ in Fig. 1(b), we can observe the mode-gap effect (shadow region) formed by mode frequency shifting due to the lattice shifting.

Then we calculate the resonance modes in the PhC DHW3 microcavity with $d_A = 0.1a$ shown in Fig. 1(a) by applying 3-D FDTD method. We find several resonance modes sustained in this microcavity, which are denoted as mode-A to -H. The relationship between normalized frequency of each resonance mode and PhC r/a ratio is shown in Fig. 2(a). We also calculate the total Q $(Q_{\rm tot})$ factors of each resonance mode when r/a ratio is 0.32 by the approaches of energy decay and Fourier harmonic analysis with Padé approximation [21], as shown in Fig. 2(b). From the simulated results, we obtain $Q_{\rm tot}$ factor of 6200 from

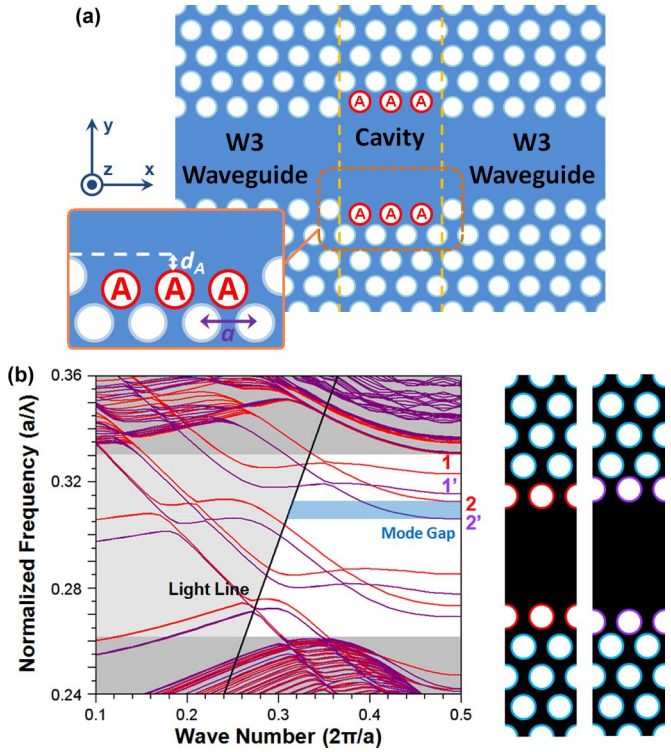

Fig. 1. (a) Scheme of PhC DHW3 microcavity based on DH structure formed by modulating the waveguide width by shifting the air-holes A. (b) Simulated TE-polarized photonic band diagram of PhC W3 waveguide without (red curves) and with (purple curves) the outward shifting of nearest six air-holes, as shown on the right. The shifting distance d_A is set to be $0.1a$. The mode gap (shadow region) is formed due to mode frequency shifting.

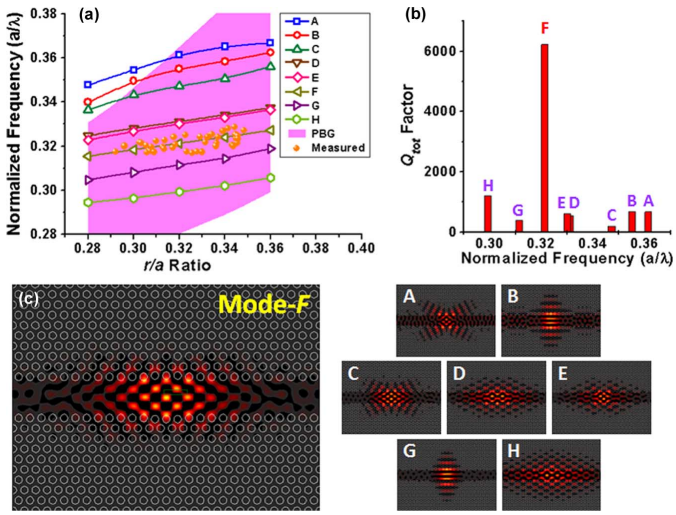

Fig. 2. (a) Relationship between the simulated resonance mode frequency and PhC r/a ratio with the air-holes shifting $d_A = 0.1a$. The PBG region and measurement results are also presented by the shadow region and solid circles. (b) The simulated $Q_{\rm tot}$ factors and (c) mode profiles in electrical-field of each resonance mode from A to H in the PhC DHW3 microcavity. High simulated $Q_{\rm tot}$ value of 6200 is obtained from mode-F.

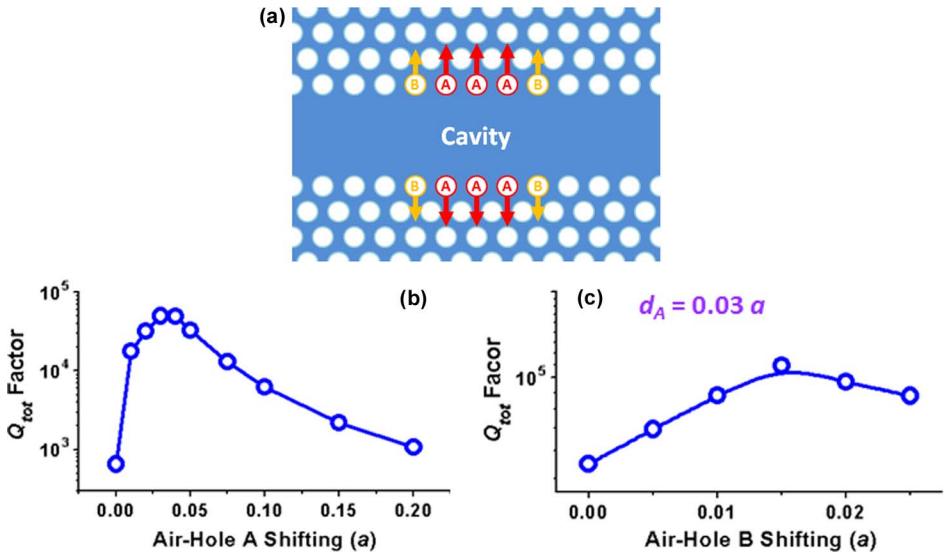

Fig. 3. (a) Scheme of optimization of PhC DHW3 microcavity by tuning the positions of air-holes A and B. (b) The simulated $Q_{\rm tot}$ factor of mode-F in PhC DHW3 microcavity when d_A is varied from 0 to $0.2a$. The highest $Q_{\rm tot}$ factor of 50 000 is obtained when d_A is $0.03a$. (c) The simulated $Q_{\rm tot}$ factor of mode-F in PhC DHW3 microcavity when d_B is varied from 0 to $0.025a$ with $d_A = 0.03a$ for further optimization. High $Q_{\rm tot}$ factor of 110 000 is obtained when d_A and d_B are $0.03a$ *and* $0.015a$, respectively.

mode-F, which is a relatively high value compared with other modes. The low $Q_{\rm tot}$ factors of other resonance modes could be attributed to the followings. Taking mode-A, -B, and -C for example, they are found to be close to the edge or even out of PBG region, which tend to be confined by index guiding rather than PBG effect and lead to the relatively low $Q_{\rm tot}$ factors. To further confirm this, the in-plane Q $(Q_{\rm in})$ factors of mode-A, -B, and -C are calculated as 890, 720, and 230, respectively, which indicate the weak PBG confinement. And the vertical Q (Q_v) factors of mode-A, -B, and -C are calculated as 2500, 6880, and 1090, respectively, which reveal the mode confinements are mainly from index guiding. On the other hand, for the cases of mode-D and -E, they are confined by mode-gap effect due to the DH structure and correspond to the frequency range between band-1 and band-1$'$ in Fig. 1(b). In this case, the simulated $Q_{\rm in}$ factors for mode-D and -E are 10 100 and 29 400, respectively, which are attributed to the PBG and mode-gap effect. However, for band-1$'$, although the mode-gap is formed, the propagating mode in the defect region can be coupled to the propagating waveguide mode in band-2. Thus, the simulated Q_v factors are only 570 and 610, respectively. In the case of high-Q mode-F, the vertical confinement is provided by index contrast and the in-plane confinement is provided by the PBG and mode-gap effect that lies between band-2 and band-2$'$. The simulated $Q_{\rm in}$ and Q_v factors are 44 000 and 7200, respectively. So far, the simulated $Q_{\rm tot}$ value from mode-F is sufficient for achieving a laser light source. However, it could be further improved for advanced quantum information processing applications.

Thus, in order to obtain higher $Q_{\rm tot}$ factor from mode-F, we optimize the cavity design by tuning the positions of air-holes A and their neighboring air-holes (yellow circles, denoted as air-holes B), as shown in Fig. 3(a). In order to keep this microcavity to be a local design, we only optimize it by tuning the air-holes A and B. First, the air-holes A are shifted outward (d_A) from 0 (original W3 waveguide) to $0.2a$. From the simulated $Q_{\rm tot}$ factors shown in Fig. 3(b), we can observe that there is a high enhanced $Q_{\rm tot}$ factor of 50 000 when d_A is $0.03a$. We then fix d_A to be $0.03a$ and further shift the air-holes B outward (d_B) from 0 to $0.025a$. The simulated $Q_{\rm tot}$ factors are shown in Fig. 3(c). From Fig. 3(c), we obtain an optimized $Q_{\rm tot}$ factor of 110 000 when d_B is $0.015a$. This shifting distance is around 7.5 nm when $a = 500$ nm, which is an achievable value for nowadays EBL technology. However, in the following fabrication and measurements, in order to observe strong in-plane laser emissions in experiments more easily, we will choose the original design by only shifting of air-holes A with lower $Q_{\rm in}$ factors.

III. Fabrications, Measurements, and Analysis

In fabrications, the epitaxial structure consisting of compressively strained InGaAsP multi-quantum-wells (MQWs) on InP substrate as the active layer with 1.55 μm central wavelength and over 200 nm broad line-width under photoluminescence is prepared. First, the 140 nm silicon-nitride (Si_3N_4) layer served as hard mask for latter etching process is deposited by plasma-enhanced chemical vapor deposition process and the polymerthylmethacrylat (PMMA) layer is spin-coated on the Si_3N_4 layer. The PhC DHW3 microcavity patterns are defined on the PMMA layer by EBL technology and transferred to the Si_3N_4 layer by reactive-ion etching process. Then the patterns are further transferred into MQWs by inductively coupled plasma dry etching process. Finally, the membrane structure is formed by HCl selective wet etching. The top-view scanning-electron-microscope (SEM) pictures of PhC DHW3 microcavity formed by shifting the air-holes A $0.1a$ outward are shown in Fig. 4(a) and (b). The fabricated lattice constant and r/a ratio are estimated to be 510 nm and 0.3, respectively. The tilted-view SEM pictures of PhC DHW3 microcavity and

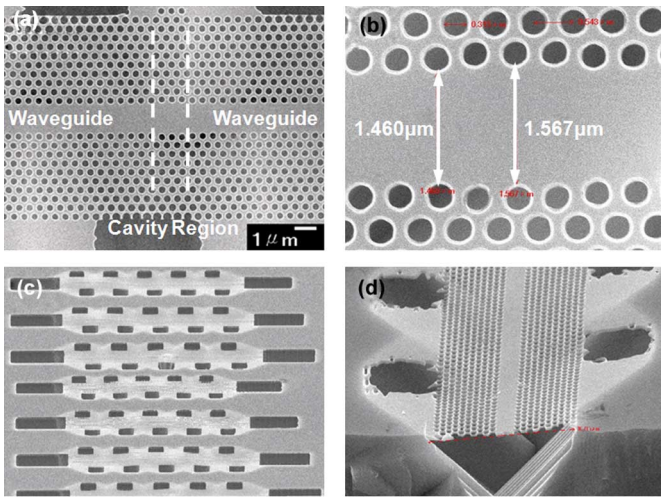

Fig. 4. (a) Top-view, (b) zoom-in, and (c) zoom-out SEM pictures of fabricated PhC DHW3 microcavities. (d) The tilted-view SEM picture of the waveguide facet of PhC DHW3 microcavity.

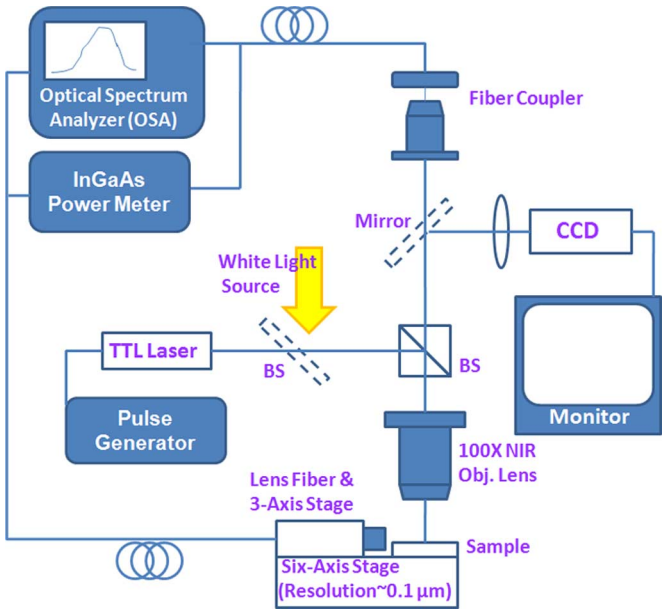

Fig. 5. Scheme of near-infrared micro-PL system setup for in-plane and vertical emissions.

its waveguide facet for in-plane emission are also shown in Fig. 4(c) and (d).

In measurements, the PhC DHW3 microcavity is optically pumped from the vertical direction by an 845-nm diode laser with 0.5% duty cycle and 25-ns pulse width. The sample is attached on a six-axial stage with high resolution of 0.1 μm. The vertically emitted light from the resonator is collected by an 100x objective lens, fed in a FC/FC multimode fiber (MMF), and then detected by an optical spectrum analyzer. At the same time, we use a lens fiber mounted on a three-axial stage to collect the in-plane emissions from the waveguide facet. This measurement setup is illustrated in Fig. 5. The measured single-mode lasing spectrum at 1593 nm and the light-in light-out $(L-L)$ curve from the vertical emission are shown in Fig. 6(a) and (b). From the $L-L$ curve and lasing spectrum, the threshold is estimated as 1.9 mW and side-mode suppression-ratio (SMSR) is larger than 23 dB, which are both better than the previously reported results by varying the whole lattice structure in [19] with the similar waveguide size. The Q factor is estimated as 3200 from the spectral line width of 0.5 nm near threshold pump level, which agrees with the simulated result ($\sim$6200) after considering fabrication imperfections. The threshold and $Q_{\rm tot}$ factor of this microcavity can be further improved according to our optimization by FDTD simulations. To confirm the collected vertical emission is from localized cavity mode lasing instead of waveguide mode emissions, we move the pump spot from position P to position P' as shown in the inset of Fig. 6(b). When the pump spot is pumped at position P, the laser emission is obtained. Once the pump spot is moved to position P', the laser emission is no longer observed, which is the direct evidence that the emission does come from the localized mode in PhC DHW3 microcavity. In the meanwhile, this also indicates the serious injected carrier scattering and absorption caused by the MQWs before carriers reaching the cavity region when the pump spot is not aligned with the microcavity. Finally, we obtain measured mode-F lasing actions from fabricated devices with different r/a ratios and the frequencies are denoted as solid circles in Fig. 2(a). Comparing them with the simulated results, we can easily address the lasing mode as mode-F.

On the other hand, we collect the in-plane emissions from the waveguide facet shown in Fig. 6(c) by a precisely controlled lens fiber. The in-plane emission also at 1593 nm is obtained from the lasing spectrum shown in Fig. 6(d). The collected intensity of in-plane emission is 20 times smaller than that of vertical emission. This can be attributed to good mode-gap confinement for in-plane direction, that is, higher $Q_{\rm in}$ of 44 000 than Q_v of 7200 from simulation, and optical loss when the radiated-light propagating from the microcavity to the waveguide facet. The latter one could be improved by reducing the unnecessary optical absorption in the waveguide region by epitaxial regrowth [17] or QW intermixing technology [22]. Besides, for the former one, in order to achieve high-efficiency in-plane output emission, the microcavity should be further studied and optimized by considering the tradeoff between the total $Q_{\rm tot}$ factor and waveguide Q (Q_{WG}) factor, that is, the lower Q_{WG} leads to higher output efficiency but lower $Q_{\rm tot}$ factor. In addition, it is also worthy to note that we do not observe any rolling-off effect due to the poor heat dissipation of air-claddings when the pump power is even larger than 3.6 mW. The possible reason is that the heat generated by localized light can dissipate effectively through the PhC waveguide itself.

To confirm above argument, we apply heat conduction analysis by FEM, which is also used in the case of 12-fold quasi-PhC microcavity we reported earlier [23]. The FEM simulation setup of PhC DHW3 microcavity is shown in Fig. 7(a). In order to accelerate the simulation, the simulation domain is reduced to be one-forth according to its axial symmetry. We also perform the simulation of 12-fold quasi-PhC microcavity with similar cavity size for comparison and its setup is shown in Fig. 7(b). In the simulation, the pulse width, duty cycle, energy level, and pump area of the heat source are set to be 25 ns, 0.5 %, 3.5 mW,

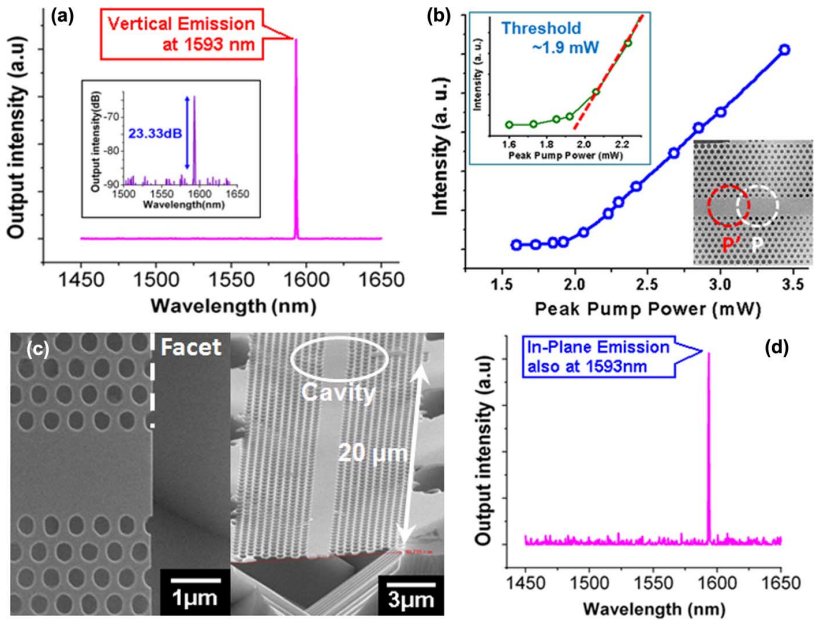

Fig. 6. (a) Typical lasing spectrum of PhC DHW3 microcavity emitted from vertical direction at wavelength of 1593 nm. The SMSR is larger than 23 dB. (b) $L-I$ curve of PhC DHW3 microcavity when the pump spot is positioned at P. The threshold is estimated to be 1.9 mW. (c) Top- (left) and tilted-view (right) SEM pictures of the waveguide facet of PhC DHW3 microcavity. The microcavity region is 20 μm away from the waveguide facet. (d) The in-plane emission spectrum collected from the waveguide facet is also at wavelength of 1593 nm.

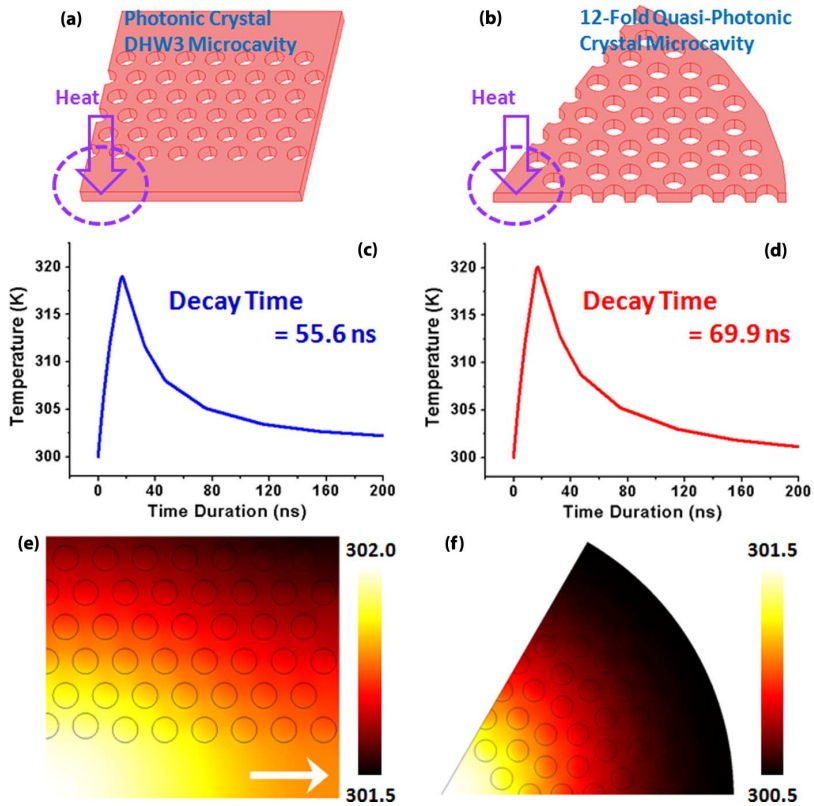

Fig. 7. FEM simulation setup of (a) PhC DHW3 microcavity and (b) 12-fold quasi-PhC microcavity. The simulated domains are reduced to be one-forth and one-sixth according to their axial symmetries. (c) (d) The simulated decay curves of microcavity temperatures versus time duration for (a) and (b). The decay times are estimated to be 55.6 and 69.9 ns, respectively. (e) (f) The simulated temperature distributions of (a) and (b) when $t = 180$ ns.

and 1.0 μm in radius, respectively. The corresponding simulated temperature decay versus time duration curves of these two microcavities are shown in Fig. 7(c) and (d). To evaluate the heat dissipation velocity in these two cases, we define a temperature decay time as the time duration for the temperature dropping to $1/e$ of its highest value. By first-order exponential fitting, the decay times are estimated to be 55.6 and 69.9 ns, respectively, which directly indicate the better heat dissipation of PhC DHW3 microcavity. Besides, according to the simulated temperature distribution shown in Fig. 7(e), we can observe that the heat flow (dissipation) is mainly through the waveguide, which is indicated by the white arrow. Thus, the waveguide connected

to the cavity region plays the role of efficient heat sink in this device indeed. For comparison, the temperature distribution of 12-fold quasi-PhC microcavity is also shown in Fig. 7(f). In 12-fold quasi-PhC microcavity, the microcavity region is surrounded by air-holes and without any significant heat dissipation pathway like the waveguide in DHW3 microcavity. Thus, a slower temperature decay time compared with that of DHW3 microcavity is obtained. Although the thermal performance of PhC microcavity is decided by various nonradiative and radiative components, when considering heat conduction merely, we can conclude this good heat dissipation property provided by the waveguide could be an important advantage of DH structure microcavity.

IV. Conclusion

In summary, we design a microcavity with in-plane and vertical emissions based on PhC waveguide with DH structure formed by locally shifting the air-holes A and B that leads to waveguide width modulation and mode-gap confinement. By PWE and 3-D FDTD calculations, we simulate and discuss the basic modal profiles and $Q_{\rm tot}$ factors of each resonance mode. After optimizing the microcavity, high simulated $Q_{\rm tot}$ factor of 110 000 is obtained from mode-F when d_A and d_B are $0.03a$ and $0.015a$, respectively. Real devices are well-fabricated by a series of dry- and wet-etching processes. The lasing emission with Q factor of 3200 and high SMSR of 23 dB at 1593 nm is obtained in vertical direction. In in-plane direction, we also observe the same lasing emission from the waveguide facet. By comparing the measured lasing actions from fabricated devices with different r/a ratios with the simulated ones, we can identify the lasing mode as mode-F. Besides, from the measured $L - L$ curve without rolling-off effect and heat transfer behaviors simulated by FEM, we can conclude that this waveguide-based microcavity has better heat dissipation than general PhC-based defect microcavities when considering thermal conduction. Finally, it should be emphasized again that this local and feasible design with the characteristic of easy-fusing with waveguide components is very benefit and promising in serving as a light sources in PICs.

Acknowledgment

The authors would like to thank the help from the Center of Nano Science and Technology (CNST), National Chiao Tung University, Taiwan.

References

[1] S. L. McCall, A. F. J. Levi, R. E. Slusher, S. L. Pearton, and R. A. Logan, "Whispering gallery mode microdisk lasers," *Appl. Phys. Lett.*, vol. 60, pp. 289–291, 1992.

[2] M. K. Seo, K. Y. Jeong, J. K. Yang, Y. H. Lee, H. G. Park, and S. B. Kim, "Low threshold current single-cell hexapole mode photonic crystal laser," *Appl. Phys. Lett.*, vol. 90, 2007, 171122.

[3] Y. Akahane, T. Asano, B. S. Song, and S. Noda, "Fine-tuned high-Q photonic crystal nanocavity," *Opt. Exp.*, vol. 13, pp. 1202–1214, 2005.

[4] K. Nozaki and T. Baba, "Lasing characteristics with ultimate-small modal volume in point shift photonic crystal nanolasers," *Appl. Phys. Lett.*, vol. 88, 2006, 211101.

[5] D. Ohnishi, T. Okano, M. Imada, and S. Noda, "Room temperature continuous wave operation of a surface-emitting two-dimensional photonic crystal diode laser," *Opt. Exp.*, vol. 12, pp. 1562–1568, 2004.

[6] S. H. Kwon, H. Y. Ryu, G. H. Kim, Y. H. Lee, and S. B. Kim, "Photonic bandedge lasers in two-dimensional square-lattice photonic crystal slabs," *Appl. Phys. Lett.*, vol. 83, pp. 3870–3872, 2003.

[7] K. Srinivasan, P. E. Barclay, M. Borselli, and O. J. Painter, "An optical-fiber-based probe for photonic crystal microcavities," *IEEE J. Sel. Areas Commun.*, vol. 23, no. 7, pp. 1321–1329, Jul. 2005.

[8] I. K. Hwang, S. K. Kim, J. K. Yang, S. H. Kim, S. H. Lee, and Y. H. Lee, "Curved-microfiber photon coupling for photonic crystal light emitter," *Appl. Phys. Lett.*, vol. 87, 2005, 131107.

[9] E. Istrate and E. H. Sargent, "Photonic crystal heterostructures and interfaces," *Rev. Mod. Phys.*, vol. 78, pp. 455–481, 2006.

[10] B. S. Song, S. Noda, T. Asano, and Y. Akahane, "Ultra-high-Q photonic double-heterostructure nanocavity," *Nature Mat.*, vol. 4, pp. 207–210, 2005.

[11] B. S. Song, T. Asano, Y. Akahane, and S. Noda, "Role of interfaces in heterophotonic crystals for manipulation of photons," *Phys. Rev. B*, vol. 71, 2005, 195101.

[12] S. H. Kwon, T. Sunner, M. Kamp, and A. Forchel, "Ultrahigh-Q photonic crystal cavity created by modulating air hole radius of a waveguide," *Opt. Exp.*, vol. 16, pp. 4605–4614, 2008.

[13] J. Topolancik, F. Vollmer, and B. Ilic, "Random high-Q cavities in disordered photonic crystal waveguides," *Appl. Phys. Lett.*, vol. 91, p. 201102, 2007.

[14] E. Kuramochi, M. Notomi, S. Mitsugi, A. Sinya, and T. Tanabe, "Ultra-high-Q photonic crystal nanocavities realized by the local width modulation of a line defect," *Appl. Phys. Lett.*, vol. 88, p. 041112, 2006.

[15] A. Shinya, S. Mitsugi, E. Kuramochi, and M. Notomi, "Ultrasmall multi-channel resonant-tunneling filter using mode gap of width-tuned photonic crystal waveguide," *Opt. Express*, vol. 13, pp. 4202–4209, 2005.

[16] S. Tomljenovic-Hanic, C. Martijn de Sterke, M. J. Steel, B. J. Eggleton, Y. Tahaka, and S. Noda, "High-Q cavities in multilayer photonic crystal slabs," *Opt. Exp.*, vol. 15, pp. 17248–17253, 2007.

[17] H. Watanabe and T. Baba, "High-efficiency photonic crystal microlaser integrated with a passive waveguide," *Opt. Exp.*, vol. 16, pp. 2694–2698, 2008.

[18] A. Sugitatsu, T. Asano, and S. Noda, "Line-defect-waveguide laser integrated with a point defect in a two-dimensional photonic crystal slab," *Appl. Phys. Lett.*, vol. 86, 2005, 171106.

[19] M. H. Shih, W. Kuang, A. Mock, M. Bagheri, E. H. Hwang, J. D. O'Brien, and P. D. Dapkus, "High-quality-factor photonic crystal heterostructure laser," *Appl. Phys. Lett.*, vol. 89, 2006, 101104.

[20] T. Yang, S. Lipson, A. Mock, J. D. O'Brien, and D. G. Deppe, "Edge-emitting photonic crystal double-heterostructure nanocavity lasers with InAs quantum dot active material," *Opt. Lett.*, vol. 32, pp. 1153–1155, 2007.

[21] W. H. Guo, Y. Z. Huang, and Q. M. Wang, "Resonant frequencies and quality factors for optical equilateral triangle resonators calculated by FDTD technique and Padé approximation," *IEEE Photon. Technol. Lett.*, vol. 12, no. 7, pp. 813–815, Jul. 2000.

[22] J. H. Marsh, "Quantum well intermixing," *Semicond. Sci. Technol.*, vol. 8, pp. 1136–1155, 1993.

[23] T. W. Lu, P. T. Lee, C. C. Tseng, and Y. Y. Tsai, "Investigation on modal properties and thermal behaviors of high quality factor 12-fold quasi-photonic crystal microcavity with different central post sizes," *Opt. Exp.*, vol. 16, pp. 12591–12598, 2008.

Chia-Ho Chen received the B.S. degree from the Department of Physics, National Chung Hsing University (NCHU), Taichung, Taiwan, in 2005 and the M.S. degree from the Display Institute, National Chiao Tung University (NCTU), Hsinchu, Taiwan, in 2007.

Recently, he has been an R&D Engineer with AU Optronics Corporation (AUO), Taiwan.

Tsan-Wen Lu received the B.S. degree from the Department of Electrical Engineering, National Tsing Hua University (NTHU), Hsinchu, Taiwan, in 2003 and the M.S. degree from the Institute of Electro-Optical Engineering, National Chiao Tung University (NCTU), Hsinchu, in 2005. Currently, he is working toward the Ph.D. degree in the Institute of Electro-Optical Engineering, NCTU.

His recent research interests are focused on III–V semiconductor-based photonic crystal microcavity laser and waveguide devices.

Po-Tsung Lee (M'06) received the B.S. degree from the Department of Physics, National Taiwan University (NTU), Taipei, in 1997 and the M.S. and Ph.D. degrees from the Department of Electrical Engineering-Electrophysics, University of Southern California (USC), Los Angeles, in 1998 and 2003, respectively. During the Ph.D. degree, she was engaged in photonic crystal microcavity lasers.

In 2003, she joined the Institute of Electro-Optical Engineering, National Chiao Tung University (NCTU), Hsinchu, Taiwan, as an Assistant Professor. In 2007, she became an Associate Professor in the Department of Photonics, NCTU. Her recent research interests are III–V semiconductor photonic crystal active and passive devices, electrical devices in display applications based on organic materials, and silicon-based solar-cell technologies.

Prof. Lee was the recipient of the University of Southern California Women in Science and Engineering (WISE) Award in 2000–2001.